ACS Photonics

Efficient Nanosecond Photoluminescence from Infrared PbS Quantum Dots Coupled to Plasmonic Nanoantennas

Gleb M. Akselrod,[†,‡] Mark C. Weidman,[‖] Ying Li,[⊥] Christos Argyropoulos,[⊥] William A. Tisdale,[‖] and Maiken H. Mikkelsen*,[†,‡,§]

[†]Center for Metamaterials and Integrated Plasmonics, [‡]Department of Electrical and Computer Engineering, and [§]Department of Physics, Duke University, Durham, North Carolina 27708, United States
[‖]Department of Chemical Engineering, Massachusetts Institute of Technology, Cambridge, Massachusetts 02139, United States
[⊥]Department of Electrical and Computer Engineering, University of Nebraska−Lincoln, Lincoln, Nebraska 68588, United States

S *Supporting Information*

ABSTRACT: Infrared (IR) light sources with high modulation rates are critical components for on-chip optical communications. Lead-based colloidal quantum dots are promising nonepitaxial materials for use in IR light-emitting diodes, but their slow photoluminescence lifetime is a serious limitation. Here we demonstrate coupling of PbS quantum dots to colloidal plasmonic nanoantennas based on film-coupled metal nanocubes, resulting in a dramatic 1300-fold reduction in the emission lifetime from the microsecond to the nanosecond regime. This lifetime reduction is primarily due to a 1100-fold increase in the radiative decay rate owing to the high quantum yield (65%) of the antenna. The short emission lifetime is accompanied by high antenna quantum efficiency and directionality. This nonepitaxial platform points toward GHz frequency, electrically modulated, telecommunication wavelength light-emitting diodes and single-photon sources.

Emission cone
Polymer shell (3 nm)
Ag nanocube L = 50-150 nm
Adhesion layer (1 nm)
Template stripped Au (50 nm)
PbS quantum dots (6.5 nm)

KEYWORDS: plasmonics, IR light sources, Purcell enhancement, quantum dots, nanoantenna, nanocube
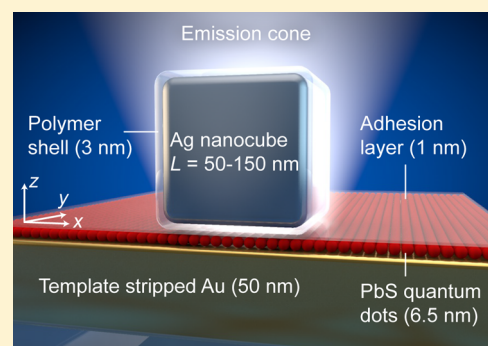
One of the ongoing challenges for on-chip optical communications is the lack of telecommunication wavelength light sources that are compatible with traditional CMOS fabrication methods. Over the past decade, light sources based on colloidal semiconductor quantum dots (QDs) have been developed, which offer advantages such as compatibility with a diverse set of substrates, wavelength tunability, and high efficiency. In particular, semiconductor quantum dots based on PbS, PbSe, and PbTe are one of the few nonepitaxial materials with high efficiency emission at near-infrared (NIR) and short-wave infrared (SWIR) wavelengths. The emission wavelength of these materials can be adjusted by simply tuning the size of the quantum dots during synthesis. To create telecommunication wavelength light sources, lead-based QDs have been used as the active material in thin-film light-emitting diodes.[1,2] With recent advances in QD synthesis and surface passivation, QD-LEDs with emission at telecommunication wavelengths have been demonstrated with efficiencies of 4.9%.[3] However, despite this progress, the ultimate limitation of QD-based IR sources for telecommunication is their slow modulation speed. Aside from electrical limitations, the fundamental limitation to modulation speed is the very slow spontaneous emission rate of PbS QDs, with typical lifetimes of several microseconds.[4] This slow radiative recombination rate is attributed to the unusual highly degenerate band structure of the QDs[5] or the

large dielectric screening of excitons in lead-based salts,[6] although the mechanism has not been entirely elucidated.

To overcome the slow intrinsic lifetime of lead-based QDs, these materials have been integrated into small mode volume optical cavities that can modify the radiative properties of emitters through the Purcell effect. The Purcell effect is the increase of the radiative and nonradiative transition rates of quantum emitters due to the increase in the local density of optical states at the location of the emitter. The Purcell factor[7] is characterized as the relative increase in the spontaneous emission rate, $F = \gamma_{sp}/\gamma_{sp}^0$, where γ_{sp} is the spontaneous emission rate in the cavity and γ_{sp}^0 is the intrinsic spontaneous emission rate. PbS QDs have been coupled to dielectric cavities such as photonic crystal cavities, achieving Purcell factors of ∼30.[8] Similarly, PbS QDs have been integrated into Si-based ring resonators, which resulted in Purcell factors of ∼13.[9] When coupled to plasmonic metamaterials, PbS QDs have been shown to have a Purcell factor of ∼100.[10] However, the role of radiative versus nonradiative decay of the QD excited state is not clear in this plasmonic metamaterial. In general, large Purcell enhancements are useful in the context of light sources only if the enhancement is primarily due to radiative rate enhancement rather than nonradiative losses in the metal.
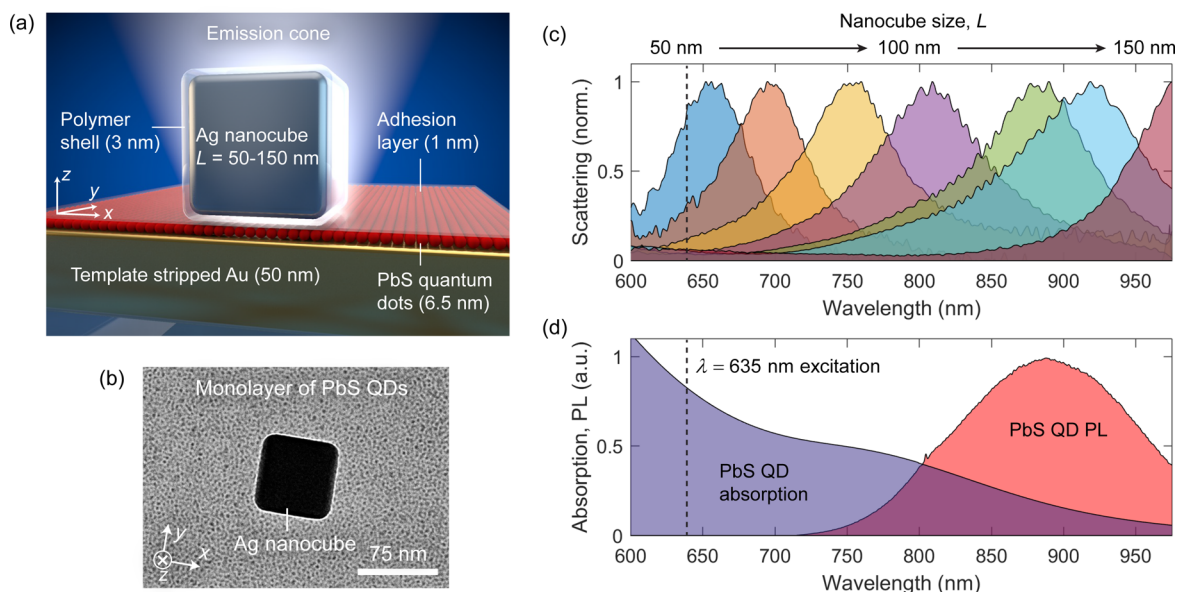
Figure 1. (a) Schematic of nanoantenna composed of a film-coupled silver nanocube with an integrated monolayer of PbS quantum dots. (b) Transmission electron microscope image of a typical nanoantenna, viewed from the top. (c) White-light scattering spectra of representative nanoantennas, with nanocube size ranging from 50 to 150 nm. (d) PbS QD absorption and emission spectra in solution. The excitation wavelength for all PL experiments was at λ_{ex} = 635 nm.

In this Letter, we demonstrate a 1300-fold enhancement in the spontaneous emission lifetime (Purcell enhancement) of PbS QDs integrated into the cavity region of a plasmonic nanoantenna. The emission lifetime is reduced from τ_0^{sol} = 2100 ns in solution to a minimum lifetime of τ = 1.6 ns, which corresponds to emission from QDs with optimal orientation and position in the nanoantenna. In addition to the lifetime reduction, the total emission intensity is dramatically enhanced due to excitation enhancement and the high quantum efficiency and directionality of the antenna. The nanoantenna consists of a colloidal silver nanocube electromagnetically coupled to a gold metal film, separated by a ~10 nm gap region into which colloidal PbS QDs are integrated (Figure 1a). The gap region forms a nanoantenna that features a high electric field enhancement (~100-fold) at the fundamental resonance. Quantum emitters coupled to this fundamental resonance have been shown to experience a large Purcell enhancement of more than 1000-fold, an effect that has been demonstrated with organic molecular dyes,[11] ensembles of visible wavelength semiconductor QDs,[12] and single QDs acting as ultrafast single-photon sources.[13] The nanoantenna structure also behaves as an efficient optical antenna with ~50% of the QD excitations coupled into free space radiation, with a single directional emission lobe.[11] Enhanced spontaneous emission in such a plasmonic system is a two-step process. First, the excited dipole (a PbS QD in this case) couples to the nanoantenna fundamental mode, generating a plasmon excitation. This plasmon can decay radiatively by emitting a photon into free space or nonradiatively by generating a hot electron via Landau damping. In our simulations, the radiative pathway occurs 65% of the time because the nanoantenna couples well to free space, as will be shown later.

The nanoantennas are fabricated entirely using bottom-up fabrication, with details described in Methods. Briefly, a thin film of gold is prepared by template stripping from an unpatterned silicon master. PbS QDs, prepared using a previously described method (average core size of 3.3 nm,

photoluminescence maximum at 888 nm),[14] are suspended in hexane and then deposited onto the surface of an acetonitrile-filled trough. As the hexane evaporates, the QDs form an ordered monolayer on the acetonitrile−air interface. The continuous monolayer is then transferred onto the template-stripped gold by dip coating the sample. The sample is then coated with a positively charged ~1 nm polymer layer to promote adhesion of nanocubes. The negatively charged nanocubes are deposited onto the sample from an aqueous solution and adhere to the sample at a low density with a typical separation of ~10 μm, such that individual nano-antennas can be addressed optically. Figure 1b shows a transmission electron microscope image of a typical nano-antenna, as viewed from the top, showing a complete monolayer of PbS QDs with a single nanocube situated above. Optical measurements on the nanoantennas are done on a custom-built microscope that allows simultaneous scattering light spectroscopy, photoluminescence (PL) spectroscopy, and time-resolved PL measurements on the same nanoparticle (see Methods).

Figure 1c shows the scattering spectra of the fundamental resonance for several representative nanoantennas. The resonance wavelength is determined by the size of the synthesized nanocube, with L = 50 nm nanocubes corresponding to a resonance of λ = 650 nm and L = 150 nm nanocubes corresponding to a resonance of λ = 925 nm. The gap between the gold top surface and silver nanocube bottom surface is set by the overall diameter of the QDs including the surface ligands (6.5 nm), the nanocube adhesion layer (1 nm), and a polymer coating on the nanocubes (3 nm). These gap parameters are kept fixed in the experiments in this study. Meanwhile, the QD emission spectrum is peaked at λ_{em} = 888 nm with a spectral width of ~150 nm, while the pulsed laser excitation is nonresonant at λ_{ex} = 635 nm (Figure 1d).

By changing the nanocube size, the nanoantenna's fundamental mode can be brought in and out of resonance with the emission of the QDs, thus controlling the Purcell

enhancement. Figure 2a shows the scattering spectra of several nanoantennas of varying size and the corresponding PL from
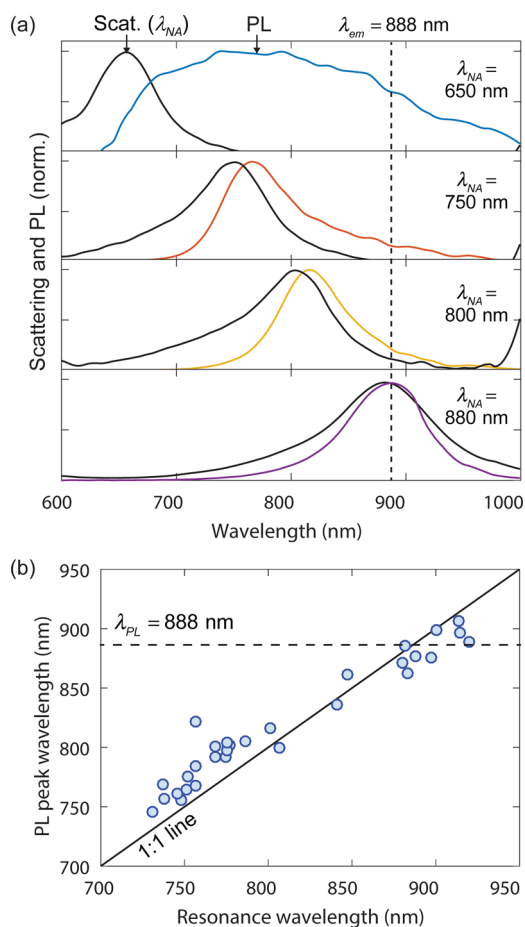
Figure 2. (a) Scattering and PL spectra for four representative nanoantennas, with scattering resonance wavelength, λ_{NA}, ranging from 650 to 880 nm. The peak QD emission wavelength, λ_{em} = 888 nm, is shown as a dashed line. (b) PL peak wavelength as a function of the scattering resonance wavelength, showing a small deviation from the 1:1 line (black line).

the embedded QDs. The PL spectrum closely follows the scattering spectrum, illustrating that the nanoantenna enhances emission from the subset of QDs that are resonant with the nanoantenna. However, the PL spectrum shows a small shift from the scattering resonance toward the intrinsic QD emission spectrum with a peak at 888 nm (Figure 2a and b). For very large detunings between the intrinsic QD emission and the nanoantenna resonance (λ_{NA} = 650 nm), very weak PL emission with a modified spectrum is observed due to poor spectral overlap.

The spectral overlap between the nanoantenna resonance and the QD emission spectrum also has a strong effect on the PL dynamics. The intrinsic QD PL in a solution of toluene is monoexponential with a lifetime of τ_0^{sol} = 2100 ns (Supporting Information Figure S1).[15] When the QDs are coupled to the nanoantenna, the emission decay dynamics are highly nonexponential with decay on the nanosecond time scale (Figure 3). The nonexponential dynamics occur because different QDs experience a Purcell effect that is dependent on their position in the nanoantenna cavity. To account for this nonexponential behavior, we fit the PL decay curves to a
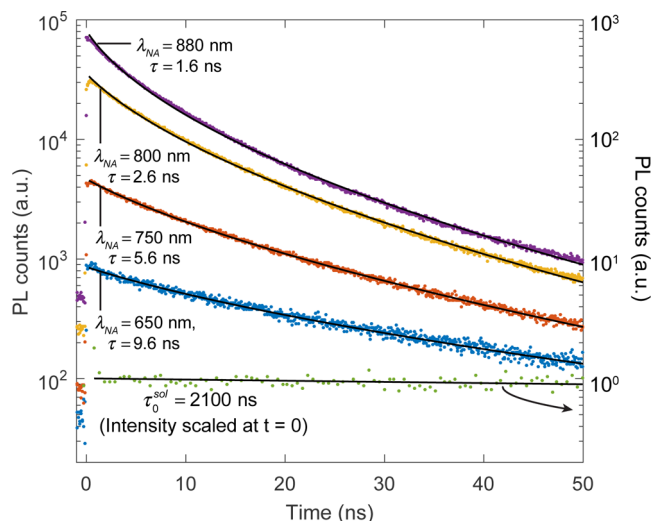

Figure 3. Time-resolved PL from four representative nanoantennas with varying resonances. The nanoantenna measurements are not normalized and were done under the same experimental conditions. Black lines are fits to a stretched exponential function, with the initial lifetime obtained from the fits shown under each curve. The intrinsic lifetime of QDs in solution is also shown and has been normalized at t = 0, for comparison with the nanoantenna data.

stretched exponential function (Figure 3). From this fit it is possible to extract the fastest decay component, corresponding to the slope of the curves at t = 0. This time constant is due to emission from optimally coupled QDs and ranges from τ = 9.6 ns for a highly detuned nanoantenna with λ_{NA} = 650 nm, increasing to τ = 1.6 ns for a nanoantenna with λ_{NA} = 880 nm, which is resonant with the QD emission. For the resonant nanoantenna, this lifetime corresponds to an enhancement in the total spontaneous emission rate relative to solution (Purcell factor) of $F = \tau_0^{sol}/\tau$ = 1300. Similarly, the emission rate enhancement can be defined relative to the lifetime of QDs in the thin film, which was measured to be τ_{tf}^0 = 420 ns, resulting in a rate enhancement of $F = \tau_0^{tf}/\tau$ = 260 (Supporting Information Figure S1). The enhancement in the radiative decay rate can then be calculated using $\gamma_r/\gamma_r^0 = (\tau_0^{sol}QY)/(\tau QY_0)$, where QY_0 is the quantum yield in solution and QY is the quantum yield of the nanoantenna emission. The solution quantum yield of the QDs was measured to be QY_0 = 76% using an integrating sphere technique (see Methods). On the basis of the lifetime of the QDs in the thin film relative to solution, the thin film quantum yield is QY_{tf} = 15%. Meanwhile, the nanoantenna quantum yield is QY = 65% across the gap region, as determined from simulation, which is discussed below. Using these quantum yield values, the estimated enhancement in the radiative rate is then γ_r/γ_r^0 = 1100.

As the spectral overlap between the QD emission and the nanoantenna resonance increases, the total amount of PL also significantly increases, as shown in the un-normalized data in Figure 3. Figure 4a shows the Purcell factor as a function of scattering resonance wavelength for ~50 nanocubes. The largest Purcell enhancements of ~1300 occur when the nanoantenna is resonant with the intrinsic emission spectrum, which is shown in the background in Figure 4a. Even larger enhancements occur at resonances beyond 900 nm, but the PL intensity at these wavelengths is significantly lower, as will be discussed below.
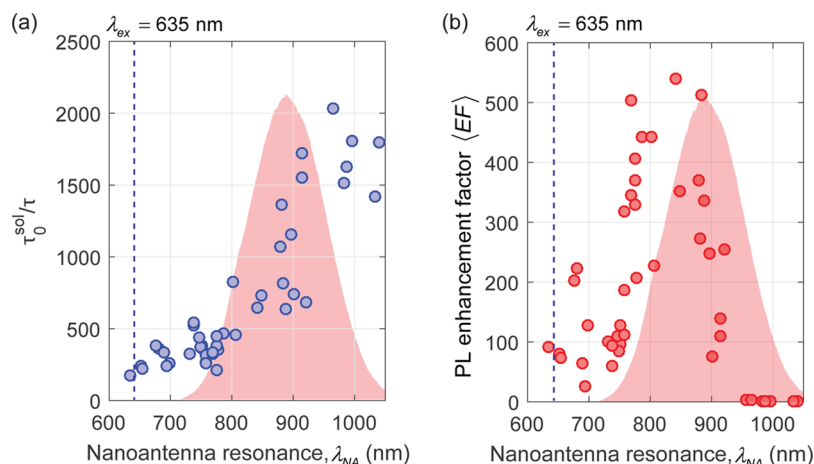
Figure 4. Purcell factor and PL enhancement factor. (a) Purcell factor as a function of nanoantenna scattering resonance wavelength. Shaded area represents the QD intrinsic emission spectrum. (b) PL enhancement factor for the same set of nanoantennas as in (a).
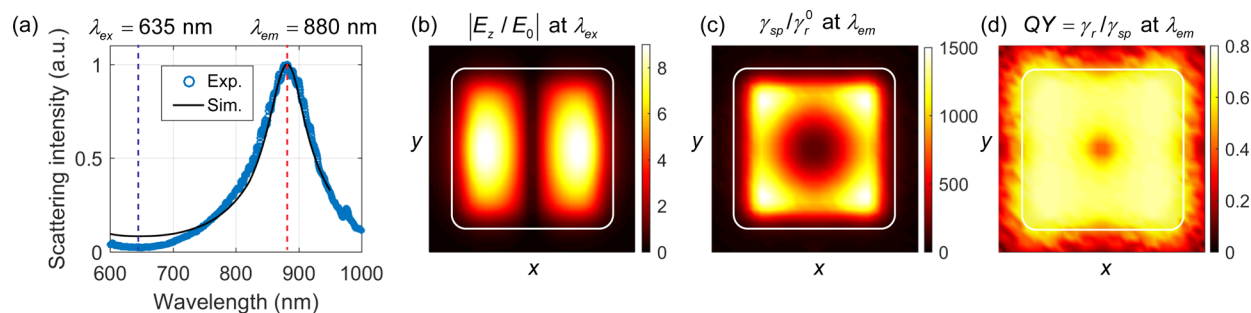
Figure 5. Simulations of nanoantenna structure. (a) Simulated scattering spectrum for a nanocube with a side length of $L = 123$ nm. Also shown is the measured scattering spectrum for a representative nanoantenna with the same resonance wavelength. (b) Spatial map in the gap region of the electric field enhancement at the excitation wavelength of $\lambda_{ex} = 635$ nm. White outline shows the lateral extent of the nanocube. (c) Spatial map of the enhancement in the total spontaneous emission rate (Purcell factor) for a dipole emitting at $\lambda_{em} = 880$ nm, resonant with the fundamental mode of the nanoantenna. (d) Spatial map of the emission quantum yield, defined as $QY = \gamma_r/\gamma_{sp}$, where γ_r is the radiative decay rate of the fundamental mode.

Simultaneous with the reduced lifetime, the time-integrated PL intensity is also substantially increased (Figure 4b). This increase can be characterized by the average PL enhancement factor per QD, which is given by $\langle EF \rangle = (I_{NA}A_{glass})/(I_{glass}A_{NA})$, where I_{NA} is the time-integrated PL from the nanoantenna and I_{glass} is the time-integrated PL intensity from a monolayer of QDs on glass. The control sample on which I_{glass} was measured consisted of a monolayer of QDs deposited directly on a glass substrate. This monolayer was prepared and deposited in the same manner as for the nanoantennas, creating a reference sample in which the QDs have the same intrinsic PL quantum yield as QDs coupled to the nanoantenna. The control sample QDs were not coated with a poly(allylamine) hydrochloride (PAH) layer. The PL intensities from the control sample and the nanoantenna are normalized for the measurement area in each case, where $A_{NA} = L^2$ is the area under the nanocube and $A_{glass} = (350 \text{ nm})^2$ is the diffraction-limited excitation spot on the control sample. Flourescence enhancement factors of up to $\langle EF \rangle = 500$ are observed for nanoantennas that are slightly blue-shifted relative to the QD emission spectrum. This shift and the origin of the enhancement in general can be understood by considering the three effects that contribute to the PL enhancement. First, there is excitation enhancement relative to free space at the laser pump wavelength of $\lambda_{ex} = 635$ nm due to overlap with the spectral shoulder of the fundamental resonance. As a result, the longer the wavelength

of the nanoantenna resonance, the weaker this overlap is, skewing the enhancement factor distribution from the QD emission peak toward the excitation wavelength. Second, the nanoantenna modifies the PL quantum yield through coupling to radiative and nonradiative decay channels of the nano-antenna.[11,16] Third, the nanoantenna modifies the radiation pattern of the emitters, and we have shown that ∼84% of the emission is collected into a high numerical aperture objective, relative to ∼18% collection efficiency for QDs on glass.[12]

The PL dynamics and PL enhancement factor can be understood more quantitatively through full-wave three-dimensional simulations of the nanoantenna structure (see Methods). The QDs in the nanoantenna gap region are modeled as a homogeneous layer 6.5 nm in thickness with a nondispersive dielectric constant of $\varepsilon = 3.25$. As the effective dielectric constant of a monolayer QD film is difficult to determine from spectroscopic ellipsometry, we used this value as a fit parameter to adjust the nanoantenna resonance wavelength from simulations to fit the experimentally observed resonance. The simulated fundamental resonance scattering spectrum for a nanoantenna with an $L = 123$ nm nanocube is shown in Figure 5a, along with a typical measured scattering spectrum for a nanocube size of ∼125 nm, as determined from SEM analysis. The width of the resonances agrees well between experiment and simulations, indicating that the QD layer can be modeled effectively as a lossless dielectric.

Figure 5b shows a map of the electric field enhancement relative to free space as a function of position under the nanocube. Despite the excitation being far from resonance, the electric field is still enhanced up to a factor of ~8, with the dipolar spatial field distribution of the fundamental mode still apparent. To calculate the emission rate enhancement, the QDs are modeled as point electric dipoles with vertical (z) orientation, and their decay rate is determined by the Green's function formalism.[16] A map of the Purcell factor, $\gamma_{sp}/\gamma_{sp}^0$, shows that dipoles located near the corners of the nanocube and having a vertical orientation experience the largest enhancements of up to 1500 (Figure 5c). This value for optimally oriented and positioned QDs is consistent with the measured maximum Purcell factor for on-resonance nanoantennas (Figure 3). At the same time, the quantum yield for emission is QY = 65% across the nanoantenna gap region (Figure 5d). This high quantum yield is consistent with experiments: the large measured ⟨EF⟩ values along with the large Purcell factors indicate that the short PL lifetime observed is not due to nonradiative quenching, but is mostly attributed to radiative rate enhancement.

In conclusion, we have demonstrated that plasmonic nanoantennas can be used to dramatically control the radiative properties of intrinsically slow near-infrared QD emitters. The nanosecond-scale emission was shown to be accompanied by a high quantum yield of emission due to the engineered structure of the nanoantenna. These emission dynamics point toward infrared light sources based on colloidal QDs with ~GHz modulation speeds, far surpassing the state of the art QD light-emitting diode performance. This nanoantenna architecture is also scalable to resonances at telecommunications wavelengths (e.g., 1500 nm), simply by synthesizing larger faceted plasmonic nanoparticles. While the present demonstration used optical excitation, the structure is in principle compatible with electrical excitation, either by using the plasmonic metal surfaces as contacts[17] or by integrating additional ultrathin and electrically active materials into the gap region.[18] The nanoantenna could also be coupled to individual infrared QDs located near the corner of the nanocube, thus resulting in high repetition rate single-photon sources at telecommunications wavelengths.

■ METHODS

PbS Nanocrystal Synthesis. Small PbS nanocrystals (~3.3 nm in diameter, as determined by transmission electron microscopy (TEM)) were synthesized according to a previously described method.[14] Briefly, 2.5 g of lead chloride (PbCl$_2$, Alfa Aesar, 99.999%) was added to 30 mL of oleylamine (Acros Organics, 80−90%) with magnetic stirring and degassed under vacuum while heating to 80 °C. At 80 °C the flask was backfilled with nitrogen and heated to 140 °C, where it was held for 30 min. The flask was then cooled to 35 °C, and 0.630 mL of bis(trimethylsilyl)sulfide (Sigma-Aldrich) was swiftly injected. The reaction proceeded for 90 s before it was stopped by the injection of cold hexane. The product was purified using a combination of methanol and butanol to precipitate the nanocrystals with centrifugation. The nanocrystals were precipitated twice and redispersed in hexane. The suspension was centrifuged again to remove any residual PbCl$_2$, which precipitated as a white powder.

Absorption and Emission. For the data in Figure 1d, absorption was collected using a Cary 5000 UV−vis−NIR spectrophotometer. The emission was wavelength-dispersed using an Acton SP2500 spectrograph (Princeton Instruments) and collected on a Pixis CCD camera. The nanocrystals were dispersed in tetrachloroethylene for both measurements.

Quantum Yield. Photoluminescence quantum yield was measured using an integrating sphere. The nanocrystals, either dispersed in tetrachloroethylene or as a thin film on glass, were excited using a 405 nm laser, and their emission was detected using a photodiode (Newport 818-UV).

Nanoantenna Fabrication. Silver nanocubes were synthesized using a previously described method.[19,20] To begin the nanoantenna fabrication, a gold film, 75 nm in thickness, was prepared by template stripping with an RMS surface roughness of 0.3 nm. The PbS QDs were resuspended in hexane at a concentration of 1 mg/mL, and 100 μL of this solution was floated on the surface of a Teflon well (1.5 × 1.5 cm) filled with acetonitrile.[21] As the hexane evaporated, the QDs formed an ordered monolayer at the acetonitrile−air surface. After 10 min, the monolayer was transferred onto the template-stripped gold by dipping the sample under the monolayer and picking it up at an angle, thus transferring the monolayer. The sample was nitrogen dried to remove excess solvent. The sample was then immersed for 5 min in a 3 mM solution of PAH and 1 M NaCl and subsequently rinsed with water. This dip-coating step forms a positively charged 1 nm adhesion layer for the nanocubes. The negatively charged nanocubes are drop cast onto the sample at a concentration of 0.01 mg/mL for 5 min, allowing the nanocubes to adhere to the sample with a mean spacing of ~10 μm, with the residual nanocubes rinsed away with water.

Optical Measurements. The optical characterization was performed using a custom microscope capable of dark-field imaging, spectroscopy, and time-resolved PL measurements on the same nanoantenna.[11] First, using a 100×, 0.9 NA microscope objective, dark-field scattering imaging is performed on the sample to identify the positions of the nanoantenna. The nanoantenna of interest is moved to the center of the field of view, and the scattered light is collected through a confocal pinhole onto a CCD spectrograph to measure the scattering spectrum. To measure the PL spectrum, the same nanoantenna is excited with a pulsed supercontinuum white light source (NKT Photonics), passing through an acousto-optic tunable filter set to 635 nm and operating at a 20 MHz repetition rate. The Gaussian output of the fiber is focused onto the nanoantenna, and the PL is passed through a 650 nm long-pass filter and spectrally resolved on a CCD spectrometer. For time-resolved measurements, the PL is sent onto a single-photon-counting avalanche photodiode connected to a time-correlated single-photon-counting system (Picoquant).

■ ASSOCIATED CONTENT

ⓢ Supporting Information

The Supporting Information is available free of charge on the ACS Publications website at DOI: 10.1021/acsphotonics.6b00357.

    Time-resolved photoluminescence data for the control samples of QDs in solution and in a thin film (PDF)

■ AUTHOR INFORMATION

Corresponding Author

*E-mail: m.mikkelsen@duke.edu.

Notes

The authors declare no competing financial interest.

ACKNOWLEDGMENTS

REFERENCES

(1) Shirasaki, Y.; Supran, G.; Bawendi, M.; Bulović, V. Emergence of colloidal quantum-dot light-emitting technologies. *Nat. Photonics* **2013**, *7*, 13−23.

(2) Supran, G. J.; Song, K. W.; Hwang, G. W.; Correa, R. E.; Scherer, J.; Dauler, E. A.; Shirasaki, Y.; Bawendi, M. G.; Bulovic, V. High-Performance Shortwave-Infrared Light-Emitting Devices Using Core-Shell (PbS-CdS) Colloidal Quantum Dots. *Adv. Mater.* **2015**, *27*, 1437−1442.

(3) Gong; Xiwen; Yang; Zhenyu; Walters; Grant; Comin; Riccardo; Ning; Zhijun; Beauregard; Eric; Adinolfi; Valerio; Voznyy; Oleksandr; Sargent, E. H. Highly Efficient Quantum Dot near-Infrared Light-Emitting Diodes. *Nat. Photonics* **2016**, *10*, 253−257.

(4) Moreels, I.; Lambert, K.; Smeets, D.; De Muynck, D.; Nollet, T.; Martins, J. C.; Vanhaecke, F.; Vantomme, A.; Delerue, C.; Allan, G.; Hens, Z. Size-Dependent Optical Properties of Colloidal PbS Quantum Dots. *ACS Nano* **2009**, *3*, 3023−3030.

(5) Saran, R.; Curry, R. J. Lead Sulphide Nanocrystal Photodetector Technologies. *Nat. Photonics* **2016**, *10*, 81−92.

(6) Wehrenberg, B. L.; Wang, C.; Guyot-Sionnest, P. Interband and Intraband Optical Studies of PbSe Colloidal Quantum Dots. *J. Phys. Chem. B* **2002**, *106*, 10634−10640.

(7) Purcell, E. Spontaneous Emission Probabilities at Radio Frequencies. *Phys. Rev.* **1946**, *69*, 681.

(8) Fushman, I.; Englund, D.; Vučković, J. Coupling of PbS Quantum Dots to Photonic Crystal Cavities at Room Temperature. *Appl. Phys. Lett.* **2005**, *87*, 241102.

(9) Humer, M.; Guider, R.; Jantsch, W.; Fromherz, T. Integration, Photostability and Spontaneous Emission Rate Enhancement of Colloidal PbS Nanocrystals for Si-Based Photonics at Telecom Wavelengths. *Opt. Express* **2013**, *21*, 18680−18688.

(10) Tanaka, K.; Plum, E.; Ou, J. Y.; Uchino, T.; Zheludev, N. I. Multifold Enhancement of Quantum Dot Luminescence in Plasmonic Metamaterials. *Phys. Rev. Lett.* **2010**, *105*, 227403.

(11) Akselrod, G. M.; Argyropoulos, C.; Hoang, T. B.; Ciracì, C.; Fang, C.; Huang, J.; Smith, D. R.; Mikkelsen, M. H. Probing the Mechanisms of Large Purcell Enhancement in Plasmonic Nanoantennas. *Nat. Photonics* **2014**, *8*, 835−840.

(12) Hoang, T. B.; Akselrod, G. M.; Argyropoulos, C.; Huang, J.; Smith, D. R.; Mikkelsen, M. H. Ultrafast Spontaneous Emission Source Using Plasmonic Nanoantennas. *Nat. Commun.* **2015**, *6*, 7788.

(13) Hoang, T. B.; Akselrod, G. M.; Mikkelsen, M. H. Ultrafast Room-Temperature Single Photon Emission from Quantum Dots Coupled to Plasmonic Nanocavities. *Nano Lett.* **2016**, *16*, 270−275.

(14) Zhang, J.; Gao, J.; Miller, E. M.; Luther, J. M.; Beard, M. C. Diffusion-Controlled Synthesis of PbS and PbSe Quantum Dots with in Situ Halide Passivation for Quantum Dot Solar Cells. *ACS Nano* **2014**, *8*, 614−622.

(15) Weidman, M. C.; Beck, M. E.; Hoffman, R. S.; Prins, F.; Tisdale, W. A. Monodisperse, Air-Stable PbS Nanocrystals via Precursor Stoichiometry Control. *ACS Nano* **2014**, *8*, 6363−6371.

(16) Ciracì, C.; Rose, A.; Argyropoulos, C.; Smith, D. R. Numerical Studies of the Modification of Photodynamic Processes by Film-Coupled Plasmonic Nanoparticles. *J. Opt. Soc. Am. B* **2014**, *31*, 2601.

(17) Sheldon, M. T.; van de Groep, J.; Brown, A. M.; Polman, A.; Atwater, H. A. Nanophotonics. Plasmoelectric Potentials in Metal Nanostructures. *Science* **2014**, *346*, 828−831.

(18) Youngblood, N.; Anugrah, Y.; Ma, R.; Koester, S. J.; Li, M. Optical Modulator and Photodetector Integrated on Silicon Waveguides. *Nano Lett.* **2014**, *14*, 2741−2746.

(19) Zhang, Q.; Li, W.; Wen, L.-P.; Chen, J.; Xia, Y. Facile Synthesis of Ag Nanocubes of 30 to 70 Nm in Edge Length with CF(3)COOAg as a Precursor. *Chem. - Eur. J.* **2010**, *16*, 10234−10239.

(20) Hoang, T. B.; Huang, J.; Mikkelsen, M. H. Colloidal Synthesis of Nanopatch Antennas for Applications in Plasmonics and Nanophotonics. *J. Visualized Exp.* **2016**, *111*, e53876.

(21) Dong, A.; Chen, J.; Vora, P. M.; Kikkawa, J. M.; Murray, C. B. Binary Nanocrystal Superlattice Membranes Self-Assembled at the Liquid−air Interface. *Nature* **2010**, *466*, 474−477.